People Detection Radar: Design and Implementation

Dissertation submitted to

Visvesvaraya National Institute of Technology, Nagpur

In partial fulfillment of the requirements for the award of the degree

Master of Technology
in
VLSI Design

by

Alok Kumar

(MT23MVD015)

Under the guidance of

Dr. Vasu Pulijala

Centre for VLSI and Nanotechnology
Visvesvaraya National Institute of Technology
Nagpur 440010 (India)

June 2025

People Detection Radar: Design and Implementation

Dissertation submitted to

Visvesvaraya National Institute of Technology, Nagpur

In partial fulfillment of the requirements for the award of the degree

Master of Technology
in
VLSI Design

by

Alok Kumar

(MT23MVD015)

Under the guidance of

Dr. Vasu Pulijala

Centre for VLSI and Nanotechnology
Visvesvaraya National Institute of Technology
Nagpur 440010 (India)

June 2025

©Visvesvaraya National Institute of Technology, Nagpur 2025

Centre for VLSI and Nanotechnology

Visvesvaraya National Institute of Technology, Nagpur

DECLARATION

I, **Alok Kumar**, hereby declare that this dissertation titled **"People Detection Radar: Design and Implementation"** is carried out by me in the **Center for VLSI and Nanotechnology** of Visvesvaraya National Institute of Technology, Nagpur. The work is original and has not been submitted earlier whole or in part for the award of any degree/diploma at this or any other Institution / University.

Alok Kumar

Date:

CERTIFICATE

This is to certify that the dissertation titled **"People Detection Radar: Design and Implementation"** is submitted by **Alok Kumar (MT23MVD015)** in partial fulfillment of the requirements for the award of **Master of Technology in VLSI Design,** VNIT Nagpur. The work is comprehensive, complete and fit for final evaluation.

Dr. Vasu Pulijala

Centre for VLSI and Nanotechnology

VNIT, Nagpur.

Prof. Sanjay B. Dhok

Head, Centre for VLSI and Technology
VNIT, Nagpur
Date:_____

Center for VLSI and Nanotechnology

Visvesvaraya National Institute of Technology, Nagpur

June 2025

Non-Plagiarism Certificate

Certified that M. Tech Dissertation titled **"People Detection Radar: Design and Implementation"** submitted by **Alok Kumar (MT23MVD015)** has been checked for plagiarism using TURNITIN software and the overlap is found within prescribed limits. A summary of the report is given below;

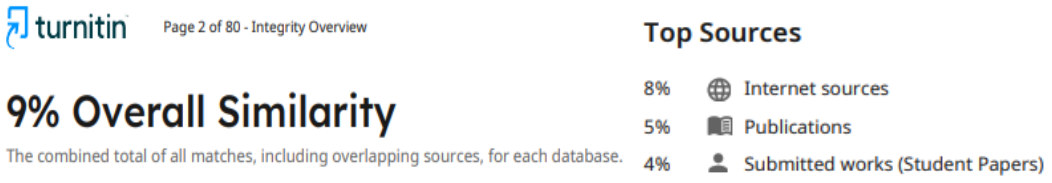
turnitin
Page 2 of 80 - Integrity Overview
9% Overall Similarity
The combined total of all matches, including overlapping sources, for each database.
Top Sources
8% Internet sources
5% Publications
4% Submitted works (Student Papers)

Figure A: Plagiarism Certificate from Turnitin Software

Alok Kumar **Dr. Vasu Pulijala**

Date: Supervisor

Acknowledgement

This research was produced with a great deal of help from many individuals, even though my name is the only one on the cover. I owe everyone who helped make my research possible my gratitude.

My deepest gratitude is to my advisor, **Dr. P.Vasu** . I have been blessed to have a mentor who allowed me the independence to research while also providing the direction I needed to correct the course when my steps stumbled. At several points during my study, I received insightful remarks and helpful criticism that led me to think and helped me narrow my focus. His tolerance and encouragement enabled me to go through several difficult situations and complete this research.

I would like to express my gratitude to **Dr. R. M. Patrikar, Dr. S. B. Dhok, Dr. R. B. Deshmukh, Dr. Nikhil Deep Gupta,** and **Dr. G. C. Patil** for their constant advice that improved my project work. I appreciate my classmates' support in keeping me motivated while I worked on my project.

I would also like to express my gratitude to The institute Director, Prof. **P. L. Patel**; Dean (Acad.) **Prof. V. R. Kalamkar** and Associate Dean (Acad - PG/PhD) **Prof. R. V. Taiwade** for their unwavering support for student academic requirements

Most importantly, none of this would have been possible without the love and patience of my family. I would like to express my heartfelt gratitude to my family.

Alok Kumar

ABSTRACT

This thesis details the design and realization of a low-frequency Frequency Modulated Continuous Wave (FMCW) radar system for non-contact human detection, leveraging Commercial Off-The-Shelf (COTS) components and embedded digital processing. The radar operates in the 1.8–2.2 GHz band and is implemented on a custom PCB integrating a voltage-controlled oscillator, low-noise amplifier, power amplifier, and supporting RF circuitry. Signal generation is accomplished using an STM32 microcontroller, which produces a linear ramp (chirp) waveform via DAC, DMA, and timer modules. To overcome the microcontroller's voltage output limitations, an analog scaling and offset circuit is employed to ensure the VCO receives the required tuning range for accurate frequency modulation.

The receiver chain digitizes the intermediate frequency (IF) signal using the STM32's ADC, and advanced digital signal processing, including FFT-based filtering, is used to extract micro-Doppler signatures. The system is tuned to detect human micro-movements such as walking gait (10–50 Hz) and stationary breathing (0.8–2 Hz), even at very low received power levels down to –38.46 dBm. Experimental results confirm the generation of clean, linear chirp signals and demonstrate reliable detection of human presence and vital signs under realistic conditions.

By combining accessible hardware with embedded signal processing, this work demonstrates that robust, real-time people detection and vital sign monitoring are achievable without reliance on expensive or proprietary radar platforms. The system's sensitivity and flexibility position it as a practical solution for healthcare, security, and smart environment applications, and provide a strong foundation for future enhancements using artificial intelligence and sensor fusion.

LIST OF FIGURES

Figure 1.1: Different Types of Human Recognition Techniques 3
Figure 3.1: Block Diagram of People Detection Radar 12
Figure 3.2: Performance Specifications of VCO 13
Figure 3.3: PAD Location and Dimension of VCO 14
Figure 3.4: Power Amplifier Specifications 15
Figure 3.5: Pin Specification of Power Amplifier 16
Figure 3.6: Layout and Circuit Diagram 16
Figure 3.7: Supply Voltage of LNA 17
Figure 3.8: Supply Current of LNA 17
Figure 3.9: Pin Specification 18
Figure 3.10: Layout of LNA 18
Figure 3.11: Relationship between Frequency, Temperature and Noise Fig. 19
Figure 3.12: PAD Location 20
Figure 3.13: PAD Location 21
Figure 4.1: Chirp Signal Output 30
Figure 5.1: Tuning Voltage for the VCO 39
Figure 6.1: DAC output measured and displayed via USART protocol on the STM board 44
Figure 6.2: Hardware validation of the ramp signal using Oscilloscope. 45
Figure 6.3: Hardware connection circuit to scale the STM board DAC output 46
Figure 6.4: Block Diagram of DAC to the Input of the VCO 46
Figure 6.5: LNA Gain (S21) 47
Figure 6.6: PCB Layout 48
Figure 6.7: PCB Measurement 53

LIST OF TABLES

Table 2.1: Comparison between Radar Types 7
Table 4.1: Output Characteristics of DAC 32
Table 5.1: Op – Amp Specification 38
Table 5.2: Performance Parameter 42
Table 6.1: S – Parameter 47
Table 6.2: Parameters 49
Table 6.3: System Losses 51

ABBREVIATIONS

ADC	Analog to Digital Converter
AI	Artificial Intelligence
CNN	Convolutional Neural Network
COTS	Commercial Off-The-Shelf
CW	Continuous Wave
DAC	Digital to Analog Converter
DMA	Direct Memory Access
dBm	Decibel-milliwatts
FFT	Fast Fourier Transform
FMCW	Frequency Modulated Continuous Wave
FSPL	Free Space Path Loss
IF	Intermediate Frequency
KNN	k-Nearest Neighbors
LFM	Linear Frequency Modulated
LNA	Low Noise Amplifier
LSTM	Long Short-Term Memory
mmWave	Millimeter Wave
NB	Naïve Bayes
OFDM	Orthogonal Frequency Division Multiplexing
Op-Amp	Operational Amplifier
PCA	Principal Component Analysis
PCB	Printed Circuit Board
PD	Pulse Doppler
RF	Radio Frequency
RMS	Root Mean Square
RCS	Radar Cross Section
SNR	Signal to Noise Ratio
STM32	STMicroelectronics 32-bit Microcontroller
SVM	Support Vector Machine
UWB	Ultra-Wideband
VCO	Voltage Controlled Oscillator

TABLE OF CONTENT

Abstract i

List of Figures ii

List of Tables iii

Abbreviations iv

INTRODUCTION 1

1.1 Background 2

1.2 Motivation 3

1.3 Thesis Organization 4

LITERATURE REVIEW 5

2. People Detection Radar 6

2.1 Evolution of Radar-Based Human Detection 6

2.2 Radar Types for Human Detection 6

2.3 Signal Processing and Artificial Intelligence Techniques 8

2.4 Applications in Healthcare and Security 8

2.5 COTS-Based Radar System Design 9

2.6 Research Gaps and Future Directions 9

HARDWARE DESIGN 10

3.1 Overview and Block Diagram 11

3.2 Power Supply and Choke 12

3.2.1 Power Supply Design 12

3.2.2 Choke Implementation 12

3.3 Voltage-Controlled Oscillator (VCO) 12

3.3.1 Component Selection and Function 12

3.3.2 Chirp Signal Generation and Control 13

3.3.3 Layout and Shielding 13

3.4 RF Signal Splitter 14

3.5 Power Amplifier 14

3.5.1 Component Selection 14

3.5.2 Biasing and Shutdown 15

3.5.3 Layout and Thermal Management 16

3.6 Low Noise Amplifier (LNA) 17

3.6.1 Component Selection 17
3.6.2 Biasing and Control 17
3.6.3 Layout 18
3.6.4 LNA GRAPH (TEMPERATURE VS FREQUENCY VS NOISE FIGURE) 19
3.7 Mixer 20
3.7.1 Layout 20
3.8 Intermediate Frequency (IF) Filter 20
3.8.1 Layout 21
3.9 Summing and Scaling Circuit (Op-Amp) 21
3.9.1 Component Selection 21
3.9.2 Circuit Design 21
3.10 PCB Layout and RF Design Considerations 21
3.10.1 Layer Stackup 21
3.10.2 Component Placement 22
3.10.3 Grounding and Shielding 22
3.10.4 Test Points and Debugging 22
3.11 Hardware Validation 22
3.11.1 Chirp Signal Verification 22
3.11.2 RF Path Testing 22
3.11.3 System Integration 22
3.12 Summary 23
SOFTWARE DESIGN 24
4.1 Introduction to Signal Processing in Radar Systems 25
4.2 Signal Type Selection and Chirp Signal Generation 25
4.2.1 Fundamental Signal Types for Radar Applications 25
4.2.2 Types of Radar Waveforms 26
4.3 Waveforms Used for Human Detection 27
4.3.1 LFM Chirp Pulses 27
4.3.2 FMCW Waveforms 27
4.3.3 UWB / Impulse Radar 28
4.4 Chirp Signal Fundamentals 28
4.4.1 Overview of Chirp Signals 28
4.4.2 Rationale for Using Chirp Signals in People Detection 29
4.4.3 Principle of Chirp Signal Operation 29

4.5 Digital-to-Analog Conversion in STM32F446RE for Radar Signal Generation 30
4.5.1 Fundamentals of DAC Operation 30
4.5.2 DAC Architecture in STM32F446RE 31
4.5.3 STM32F446RE DAC Configuration 31
4.5.4 Expected DAC Output 32
4.5.5 Code Example: Ramp Generation 32
4.5.6 Applications in Radar Systems 33
HARDWARE SOFTWARE INTEGRATION 34
5.1 Software-Hardware Integration Architecture 35
5.1.1 System Overview and Signal Flow 35
5.1.2 DAC Configuration and Optimization 35
5.1.3 Amplification Stage Design 37
5.1.4 DC Offset and Summing Circuit 38
5.1.5 VCO Integration and Frequency Validation 40
5.1.6 System Integration and Performance Validation 41
5.1.7 Summary and Key Achievements 42
RESULT 43
6.1 Simulation Result 44
6.2 Hardware Connection 45
6.3 Hardware result 47
6.3.1 S parameter 47
6.4 PCB LAYOUT 48
6.5 RECEIVED POWER USING LINK BUDGET FORMULA 49
6.5.1 Frequency & Radar Setup 49
6.5.2 Datasheet-Based Component Parameters 49
6.5.3 Free Space Path Loss (FSPL) Calculation 50
6.5.4 System Losses (Lsys) 51
6.5.5 Final Link Budget Calculation 51
6.5.6 Amplified Signal Power 51
6.5.7 Heartbeat Detection Justification 52
6.6 SUMMARY 52
6.7 PCB MEASUREMENT 53
CONCLUSION & FUTURE SCOPE 54

7.1 Conclusion 55
7.2 Future Scope 56
REFERENCES 57

1

INTRODUCTION

1.1 Background

Radar technology has become a vital tool in modern sensing applications, enabling reliable detection and monitoring in fields such as healthcare, security, and smart environments. Frequency-Modulated Continuous Wave (FMCW) radar, in particular, is valued for its ability to simultaneously measure distance and velocity, making it suitable for tracking human movement and monitoring vital signs. While most contemporary research and commercial systems for people detection have focused on millimeter-wave (mmWave) radar bands, these high-frequency solutions often require specialized components and complex design, resulting in higher costs and increased system complexity.

In contrast, this thesis explores the development of a low-frequency FMCW radar system operating in the 1.8–2.2 GHz range. This frequency band allows the use of widely available Commercial Off-The-Shelf (COTS) components, simplifies hardware design, and provides sufficient penetration and coverage for indoor environments. The system is designed to utilize chirp signals for frequency modulation, and micro-Doppler analysis to extract subtle motion signatures such as walking gait and physiological activities like breathing and heartbeat. This approach supports non-contact monitoring, which is especially valuable in privacy-sensitive applications.

Problem Statement

Despite the advantages of radar sensing, the implementation of a high-sensitivity, real-time people detection and vital sign monitoring system using cost-effective, low-frequency COTS components remains a challenge. Most existing solutions either lack the sensitivity to detect subtle physiological signals at lower frequencies or require complex, high-frequency hardware that increases system cost and design difficulty. The central problem addressed in this thesis is:

To design, implement, and validate a low-frequency FMCW radar system using COTS components and chirp signal generation, capable of reliably detecting human presence and subtle physiological activities (such as heartbeat and breathing)

in real time.

The system must integrate custom PCB hardware, embedded STM32-based signal generation and acquisition, and advanced digital signal processing for micro-Doppler analysis, ensuring practical applicability for non-contact monitoring at low received power level.

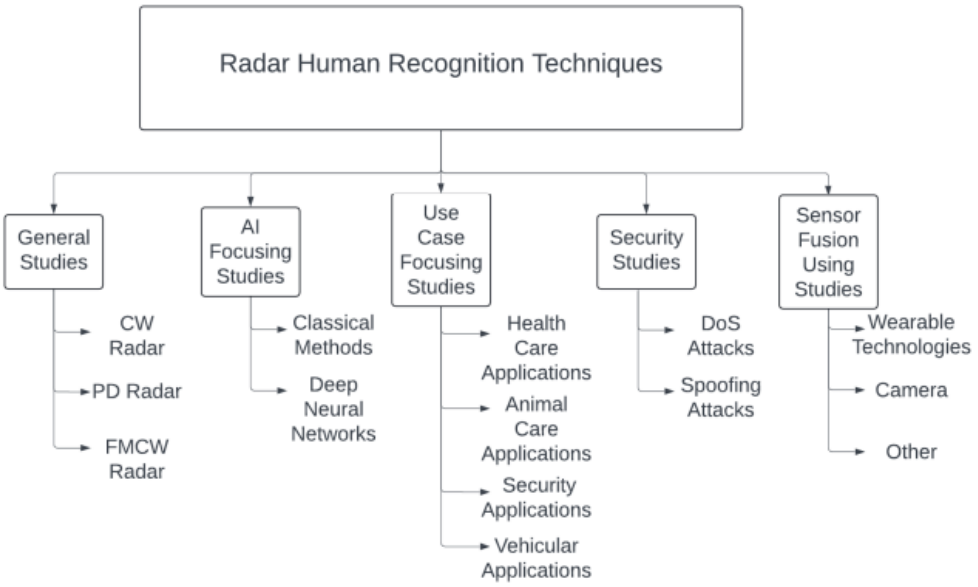

Figure 1.1: Different Types of Human Recognition Techniques[1]

1.2 Motivation

There is a growing demand for unobtrusive, privacy-preserving, and robust human detection solutions for applications such as patient monitoring, elderly care, and security. Camera-based systems, while common, are limited by privacy concerns, lighting conditions, and their inability to operate through obstacles. Wearable sensors, though effective, require user compliance and may not be suitable for continuous or long-term monitoring. Radar-based systems overcome these limitations by enabling contactless detection and classification of human activity in a wide range of environmental conditions.

However, most high-performance radar systems for people detection rely on mmWave frequencies and proprietary hardware, which can be expensive and less

accessible. By leveraging a low-frequency FMCW radar architecture using COTS components, this project aims to provide a cost-effective and practical alternative, demonstrating that reliable people detection and vital sign monitoring can be achieved without the need for high-frequency or specialized hardware. The use of chirp signal generation and micro-Doppler processing further enhances the system's ability to detect both gross and subtle human movements, making it a versatile solution for real-world scenarios.

1.3 Thesis Organization

Thesis is structured as follows:

- **Introduction:** Presents the background, motivation, and problem statement, highlighting the unique focus on low-frequency, COTS-based FMCW radar for people detection.
- **Literature Survey:** Reviews the evolution of radar-based human detection, including foundational work, recent advances in FMCW radar, micro-Doppler analysis, and the use of COTS components at low frequencies.
- **Hardware Design:** Details the custom PCB layout, component selection (including VCO, LNA, power amplifier, and op-amp), and the rationale for operating in the 1.8–2.2 GHz frequency range.
- **Software Design:** Describes the STM32-based chirp signal generation, signal acquisition, and digital processing pipeline for extracting micro-Doppler features and filtering noise.
- **Integration of Hardware and Software:** Explains the synchronization and calibration of hardware and software, as well as the procedures for system testing and validation.
- **Results:** Presents hardware verification (including PCB and oscilloscope waveform analysis), received power measurements, and detection performance for walking gait and heartbeat signals.
- **Conclusion and Future Work:** Summarizes the main contributions and discusses potential enhancements, such as advanced AI-based classification, sensor fusion, and further miniaturization.

2

LITERATURE REVIEW

2. People Detection Radar

2.1 Evolution of Radar-Based Human Detection

Radar-based human detection has seen significant growth over the past two decades, with early research primarily exploring the feasibility of using micro-Doppler radars for recognizing human activities. Initial studies, such as those by Lai, demonstrated the potential of random noise micro-Doppler radar for monitoring people inside buildings, laying the foundation for non-intrusive surveillance and security applications. Subsequent work by Tahmoush and Silvious focused on distinguishing humans from animals using Doppler radar signals, showing that features like trunk movement and limb motion could be reliably extracted for classification. These foundational studies established the viability of radar for human recognition and inspired further research into the extraction and analysis of micro-Doppler signatures.

As the field matured, researchers shifted from feasibility assessments to more utilized Support Vector Machine (SVM) classifiers to differentiate between activities such as sophisticated applications, including human behavior classification. For example, Bryan et al. walking, running, sitting, and crawling using Doppler radar traces. This progression highlighted both the promise and the challenges of radar-based human activity recognition, particularly regarding orientation dependence and reduced performance for lateral movements.

2.2 Radar Types for Human Detection

Different radar architectures offer unique capabilities for human detection:

2.2.1 Continuous Wave (CW) Radar:

CW radars transmit at a fixed frequency and are widely used for motion detection. Studies by Fioranelli et al. leveraged Multiple-Input Single-Output (MISO) CW radar to distinguish between armed and unarmed individuals by analyzing hand movement patterns during walking. CW radars have also been applied to animal care, such as detecting lameness in livestock.

2.2.2 Pulse Doppler (PD) Radar:

PD radars transmit pulses and can measure both speed and distance of moving and stationary targets. They are valued for their high resolution and ability to detect stationary objects. Shituru et al. demonstrated the use of UWB pulse-Doppler radar for non-contact measurement of heart rate and breathing, confirming its suitability for vital sign monitoring. However, PD radars face challenges in real-time applications due to processing speed limitations.

2.2.3 Frequency-Modulated Continuous Wave (FMCW) Radar:

FMCW radars, which transmit frequency-modulated chirp signals, have become increasingly popular for human detection due to their ability to measure range and velocity simultaneously. Bhattacharya et al. introduced an FMCW radar system with a CNN-based RadarNet architecture for fall detection, highlighting the potential of deep learning in radar signal processing. Vandermissen et al. demonstrated the use of FMCW radar for individual identification and gesture recognition in indoor environments, showcasing the versatility of this approach.

Table 2.1: Comparison between Radar Types

Feature/Aspect	CW Radar	FMCW Radar	Pulse Doppler Radar
Principle	Transmits a continuous, unmodulated signal	Transmits a continuous signal with frequency sweep	Transmits short, periodic RF pulses
Range Measurement	Not possible (no timing info)	Yes, via frequency difference (beat frequency)	Yes, via time delay of pulse returns
Velocity Measurement	Yes, via Doppler shift	Yes, via Doppler shift and beat frequency	Yes, via Doppler shift in pulse returns
Resolution	Good velocity, poor range	Good range and velocity	High range and velocity (with proper processing)

2.3 Signal Processing and Artificial Intelligence Techniques

Early radar-based human detection systems relied on statistical methods for activity classification. Chen et al. provided a mathematical foundation for micro-Doppler effects and validated their findings through simulations and experiments. Later, Independent Component Analysis (ICA) and Hough Transform were used for gait analysis and noise-robust moving target classification, respectively.

As the field evolved, classical machine learning techniques such as SVM, Naive Bayes (NB), k-Nearest Neighbors (KNN), and Principal Component Analysis (PCA) became standard for radar data classification. However, since 2018, there has been a marked shift towards deep learning approaches, which offer improved robustness and broader applicability. Gurbuz and Amin explored deep learning models for classifying activities in nursing home scenarios, and Li et al. used Bi-directional LSTM networks for continuous human activity detection using FMCW radar data, eliminating the need for sliding window segmentation.

Recent studies have also focused on advanced preprocessing and data augmentation techniques. Dadon et al. utilized Short-Time Fourier Transform (STFT) and Fast Fourier Transform (FFT) as preprocessing steps before CNN-based classification, while Kim et al. combined YOLO and SVM algorithms for enhanced detection performance in FMCW radar data.

2.4 Applications in Healthcare and Security

Radar-based human detection has found significant applications in healthcare, particularly for elderly care and vital sign monitoring. Fall detection is a critical use case, with Bhattacharya et al. demonstrating the effectiveness of CNN architectures for detecting falls using FMCW radar data.

Sensor fusion, such as combining radar with wearable IMU sensors, has been shown to improve classification accuracy for complex activities.

For vital sign monitoring, UWB pulse-Doppler and FMCW radars have been successfully used to detect breathing and heartbeat without physical contact, providing a non-intrusive alternative to traditional monitoring systems. These capabilities are

especially valuable in medical environments where continuous, non-contact monitoring is required.

In security applications, radar technology enables surveillance and threat assessment without the privacy concerns associated with cameras. Studies have demonstrated the ability to detect concealed weapons, distinguish between humans and animals, and identify individuals based on gait signatures.

2.5 COTS-Based Radar System Design

A notable trend in recent research is the use of Commercial Off-The-Shelf (COTS) components for radar system design, making advanced radar sensing more accessible and affordable. For example, Villeval et al. used automotive-standard Doppler radar modules for human detection in noisy urban environments, while Dadon et al. developed a CNN-based presence detection system using low-cost FMCW radar modules. These studies confirm that high performance can be achieved with readily available components, supporting the practical implementation of radar systems like the one described in this thesis.

2.6 Research Gaps and Future Directions

Despite substantial progress, several challenges remain. Radar-based human detection systems must contend with signal interference, noise, and classification accuracy degradation due to target orientation and distance.

Real-time processing on embedded platforms is another ongoing challenge, particularly for systems that must operate at low received power levels, as in this thesis. Emerging research directions include the integration of radar with other sensing modalities (such as cameras and wearables), the application of advanced AI models for more nuanced classification, and the miniaturization of radar hardware for portable and ubiquitous deployment. The continued development of COTS-based radar systems is expected to further democratize access to advanced sensing technologies.

3

HARDWARE DESIGN

3.1 Overview and Block Diagram

The radar hardware is the foundation of the people detection and vital sign monitoring system. The design is based on a modular approach, with each functional block optimized for performance, cost, and ease of integration using Commercial Off-The-Shelf (COTS) components. The main blocks are:

- Power Supply and Choke
- Voltage-Controlled Oscillator (VCO)
- RF Signal Splitter
- Power Amplifier
- Low Noise Amplifier (LNA)
- Mixer
- Intermediate Frequency (IF) Filter
- Summing and Scaling Circuit (Op-Amp)
- PCB Layout and RF Considerations

Block Diagram:

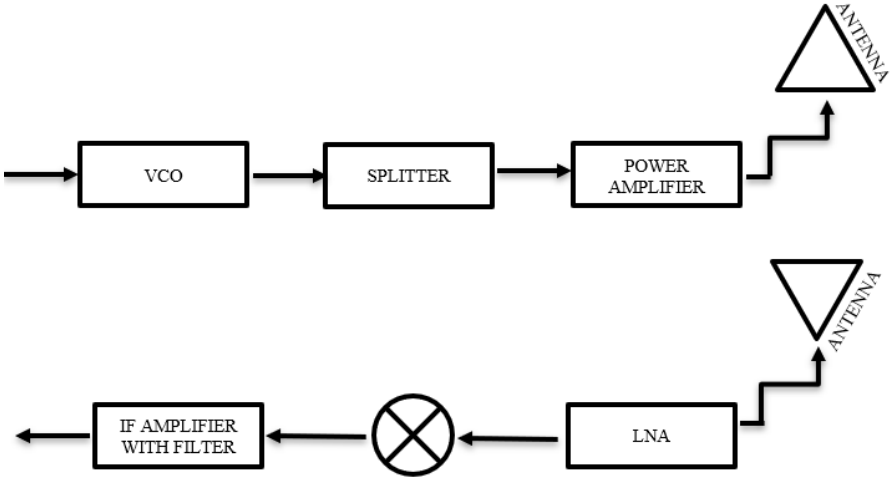

Figure 3.1: Block Diagram of People Detection Radar

3.2 Power Supply and Choke

3.2.1 Power Supply Design

A stable, low-noise power supply is essential for RF systems to minimize phase noise and interference. The radar board operates from a regulated 5V supply, distributed to all active components. High-frequency decoupling capacitors (0.1 μF and 10 μF in parallel) are placed close to each IC to suppress switching noise and voltage transients.

3.2.2 Choke Implementation

A bias choke is used to isolate the RF path from the DC supply, preventing RF leakage and ensuring clean DC biasing. The choke is chosen for high impedance at the radar's operating frequency (1.8–2.2 GHz), minimizing signal loss and ensuring proper operation of the VCO and amplifiers.

3.3 Voltage-Controlled Oscillator (VCO)

3.3.1 Component Selection and Function

The Crystek CVCO55BE-1530-2700 VCO is selected for its wide tuning range (1.53–2.7 GHz), low phase noise, and compatibility with a 5V supply2. The VCO

generates the primary RF signal for the radar, with output power typically +7.5 dBm. Its frequency is controlled by a tuning voltage, enabling frequency sweeps (chirps) for FMCW operation.

CRYSTEK MICROWAVE
A Division of Crystek Corporation

Voltage Controlled Oscillator-VCO
CVCO55BE-1530-2700

PERFORMANCE SPECIFICATION	MIN	TYP	MAX	UNITS
Lower Frequency:			1530	MHz
Upper Frequency:	2700			MHz
Tuning Voltage:	0.5		10.5	VDC
Supply Voltage:	4.75	5.0	5.25	VDC
Output Power:	+4.0	+7.5	+11.0	dBm
Supply Current:		15	30	mA
Harmonic Suppression (2nd Harmonic):		-15		dBc
Pushing:			25.0	MHz/V
Pulling, all Phases:			35.0	MHz pk-pk
Tuning Sensitivity:		140		MHz/V
Phase Noise @ 10kHz offset:		-87		dBc/Hz
Phase Noise @ 100kHz offset:		-110		dBc/Hz
Load Impedance:		50		Ω
Input Capacitance:			50	pF
Operating Temperature Range:	-40		+75	°C
Storage Temperature Range:	-45		+90	°C

RoHS Compliant

Figure 3.2: Performance Specifications of VCO[5]

3.3.2 Chirp Signal Generation and Control

The VCO is driven by a ramp voltage generated by the STM32 DAC, which is scaled and offset using an op-amp circuit to achieve the required 3.13–5.93 V tuning range.

This produces a linear frequency sweep from 1.8 GHz to 2.2 GHz, as shown in the oscilloscope waveform (Figure 3.2). The linearity and stability of this ramp are critical for accurate range and Doppler measurements.

3.3.3 Layout and Shielding

The VCO is placed close to the RF ground plane, with short, wide traces for the RF output and supply lines. Multiple vias connect the ground pad to the main ground plane, reducing inductive noise coupling.

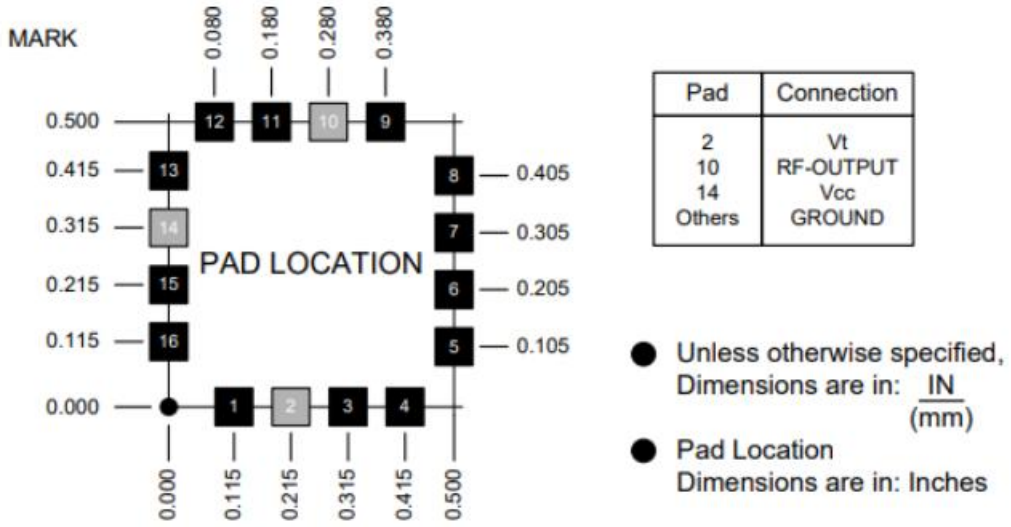

Figure 3.3: PAD Location and Dimension of VCO[5]

3.4 RF Signal Splitter

A broadband Wilkinson splitter is used to divide the VCO output into two paths: one for transmission and one for mixing (local oscillator input). The splitter is implemented with microstrip lines or a commercial integrated device, ensuring equal amplitude and phase balance. Careful impedance matching (50 Ω) and minimal trace length are maintained to reduce insertion loss and phase errors.

3.5 Power Amplifier

3.5.1 Component Selection

The Qorvo QPA9442 is chosen for its high linearity, wide frequency coverage (0.6–2.8 GHz), and ability to deliver up to 19 dB gain in the 1.8–2.2 GHz band4. It operates from a single 5V supply and can provide robust output power for effective signal transmission.

Electrical Specifications – 1.8 - 2.2 GHz Reference Design

Parameter	Conditions (1)	Min	Typ	Max	Units
Operational Frequency Range		1800		2200	MHz
Gain	At 1840MHz	14.2	15.5		dB
	At 2140MHz	14.0	15.3		dB
	At 1840MHz at +115°C	13.2			dB
	At 2140MHz at +115°C	13.0			dB
Gain Flatness (2)	Fc ± 100MHz		±0.25		dB
Input Return Loss			12		dB
Output Return Loss			15		dB
Output P1dB	At 1840MHz	27.7	28.4		dBm
	At 2140MHz	28.7	29.9		dBm
	At 1840MHz at +115°C	27			dBm
	At 2140MHz at +115°C	28			dBm
Output IP3	Pout=+10dBm/tone, Δf=1MHz, at 1840MHz	41.4	43.7		dBm
	Pout=+10dBm/tone, Δf=1MHz, at 2140MHz	40.0	43.7		dBm
ACPR	20MHz LTE TM1.1, PAR 8.5dB, Pout = +17dBm		-55		dBc
Noise Figure (3)	Over frequency and process		5.7		dB
	Over frequency and process at -40°C			5.5	dB
	Over frequency and process at +115°C			7.8	dB
Power dissipation	Pout = +10dBm, CW		1.15	1.4	W
Device Current, OFF	V_{PD} = 0 V			2	mA
V_{PD}, Logic Low		0		0.63	V
V_{PD}, Logic High		1.17		V_{CC}	V
Device ON or OFF Timing			0.26	1	µS
Thermal Resistance, θ_{jc}	Junction to case		31		°C/W

Figure 3.4: Power Amplifier Specifications[2]

3.5.2 Biasing and Shutdown

The amplifier includes a shutdown control pin (Vpd) for power management. Proper biasing is ensured using recommended resistor and inductor values from the datasheet. Decoupling capacitors are placed close to the supply pins to minimize noise.

Functional Block Diagram

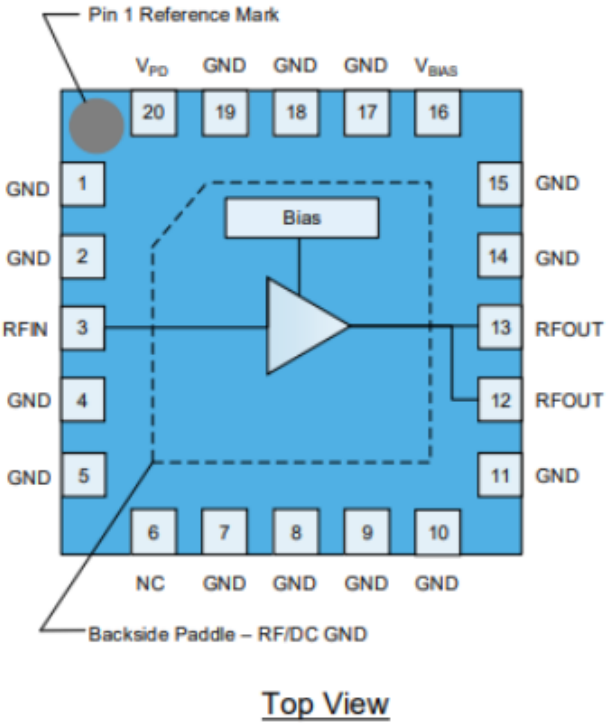

Figure 3.5: Pin Specification of Power Amplifier[2]

3.5.3 Layout and Thermal Management

The power amplifier is located near the splitter output, with short traces to minimize losses. A solid ground plane and thermal vias under the package ensure efficient heat dissipation and RF grounding.

Evaluation Board, 1800 – 2200 MHz Reference Design

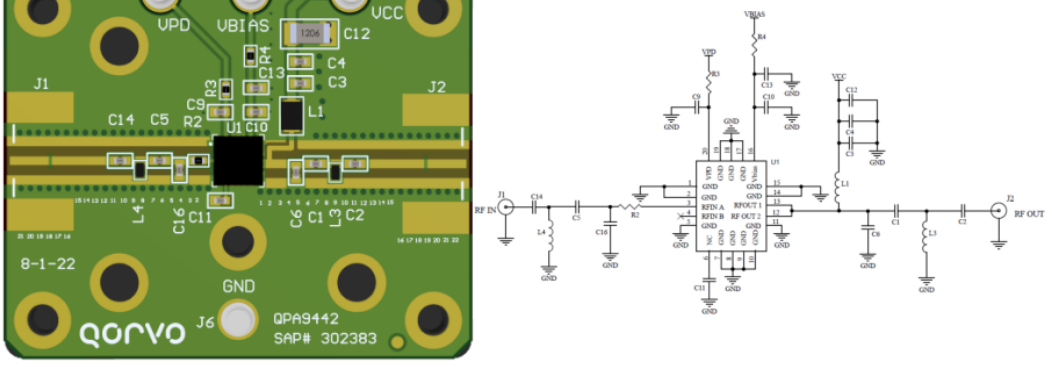

Figure 3.6: Layout and Circuit Diagram[2]

3.6 Low Noise Amplifier (LNA)

3.6.1 Component Selection

The Guerrilla RF GRF2081 is selected for its ultra-low noise figure (0.4 dB typical), high gain (18.5 dB), and broadband operation (0.7–2.7 GHz). The LNA is critical for boosting weak received signals before mixing, directly impacting the radar's sensitivity and detection range.

Recommended Operating Conditions

Parameter	Symbol	Specification			Unit	Condition
		Min.	Typ.	Max.		
Supply Voltage	V_{DD}	2.7	5	6	V	
Operating Temperature (Package Base)	$T_{PKG\ BASE}$	-40		105	°C	
RF Frequency Range	F_{RF}	0.7	1.9	2.7	GHz	Typical application schematic with external matching components **(notes 1 & 2)**.

Figure 3.7: Supply Voltage of LNA[4]

Nominal Operating Parameters – General

The following conditions apply unless noted otherwise: Typical application schematic using the 1.7 to 2.7 GHz tuning set, V_{DD} = 5 V, $V_{SHUTDOWN}$ = < 0.2 V, I_{DD} = 75 mA, F_{TEST} = 1.9 GHz, $T_{PKG\ BASE}$ = 25 °C. Evaluation board losses are included within the specifications.

Parameter	Symbol	Specification			Unit	Condition
		Min.	Typ.	Max.		
Supply Current	I_{DD}	50	75	95	mA	V_{DD} = 5 V, $V_{SHUTDOWN}$ = 0 V.
Switching Rise Time	T_{RISE}		100		ns	Disabled mode to Gain mode **(note 3)**.
Switching Fall Time	T_{FALL}		100		ns	Gain mode to Disabled mode **(note 4)**.
Thermal Data						
Thermal Resistance (Infrared Scan)	Θ_{JC}		60		°C/W	On standard evaluation board **(note 5)**.

Figure 3.8: Supply Current of LNA[4]

3.6.2 Biasing and Control

The LNA operates at 5V and 75 mA. It features a shutdown mode for power saving, controlled by the Vshutdown pin. Input and output matching networks are implemented for optimal noise and gain performance.

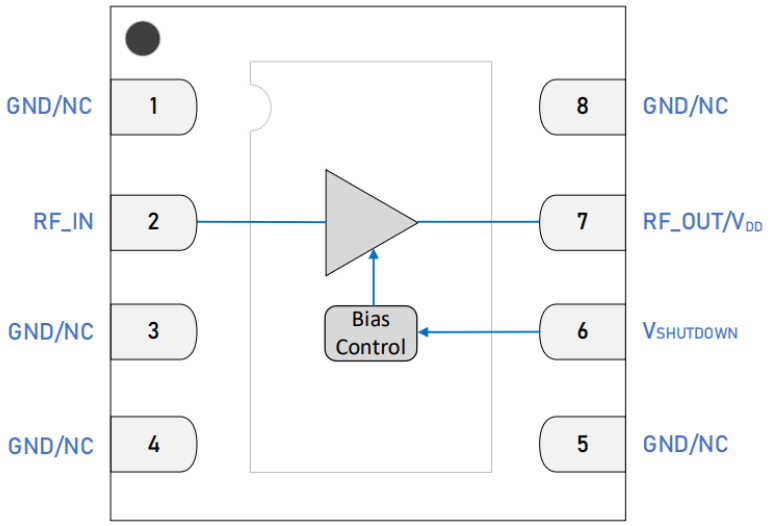

Figure 3.9: Pin Specification[4]

3.6.3 Layout

The LNA is placed close to the antenna input to minimize noise pickup and signal loss. The ground pad is connected with multiple vias, and the RF traces are kept short and shielded.

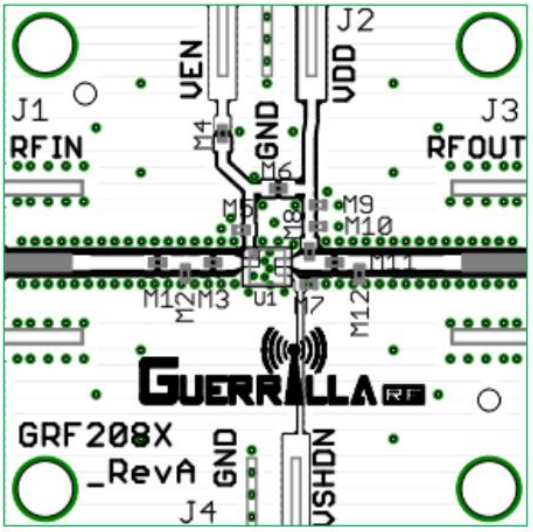

Figure 3.10: Layout of LNA[4]

3.6.4 LNA GRAPH (TEMPERATURE VS FREQUENCY VS NOISE FIGURE)

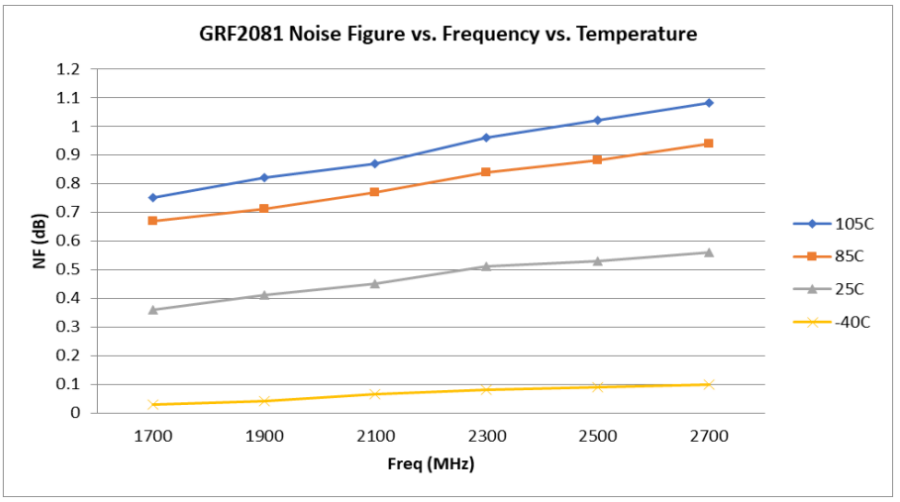

Figure 3.11: Relationship between Frequency, Temperature and Noise Fig.[4]

The graph illustrates the relationship between the noise figure (NF), frequency, and temperature for the GRF2081 device. The noise figure, measured in decibels (dB), is plotted on the vertical axis, while frequency in megahertz (MHz) is shown on the horizontal axis. Four curves represent device performance at different temperatures: -40°C, 25°C, 85°C, and 105°C.

As the frequency increases from 1700 MHz to 2700 MHz, the noise figure rises for all temperature levels. At each frequency point, higher temperatures correspond to a higher noise figure. For example, at 105°C, the noise figure starts around 0.75 dB at 1700 MHz and climbs to over 1.0 dB at 2700 MHz. In contrast, at -40°C, the noise figure remains extremely low, starting near 0.03 dB and increasing only slightly across the frequency range.

This trend demonstrates that both higher operating temperatures and higher frequencies lead to greater noise generation within the device. The increase in noise figure with temperature is due to increased thermal noise, while higher frequencies activate additional noise mechanisms.

Thus, minimizing temperature and operating at lower frequencies are effective strategies for achieving a lower noise figure in sensitive RF applications1.

3.7 Mixer

The mixer combines the received RF signal (amplified by the LNA) with the LO signal (from the VCO via the splitter) to produce an IF signal. A double-balanced mixer topology is used for its superior isolation and spurious rejection. Input and output matching networks are designed for 50 Ω impedance, and the LO drive level is set according to the mixer's requirements.

3.7.1 Layout

The mixer is centrally located between the LNA and IF filter. LO, RF, and IF traces are routed orthogonally to minimize crosstalk, and the mixer's ground is connected to the main RF ground plane.

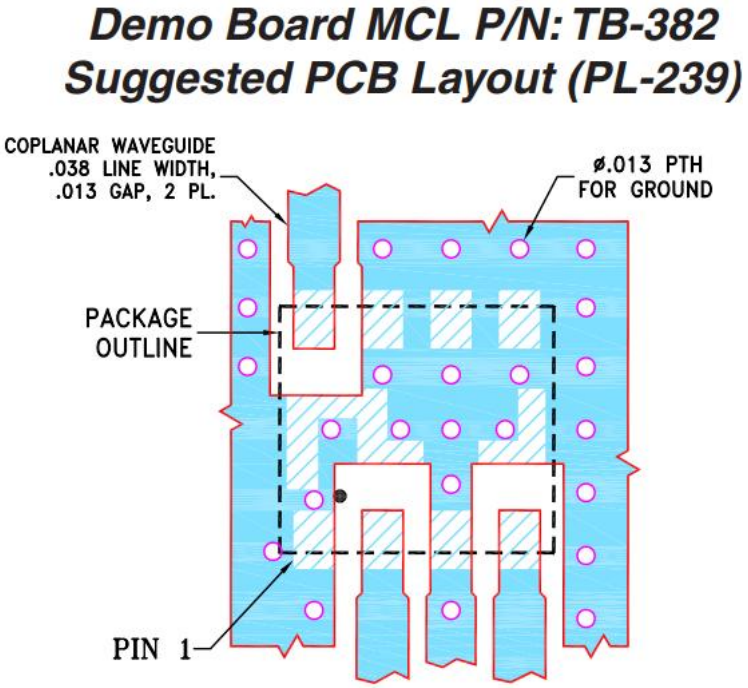

Figure 3.12: PAD Location[16]

3.8 Intermediate Frequency (IF) Filter

The IF filter removes unwanted mixer products and high-frequency noise, passing only the desired IF band to the ADC. A low-pass or band-pass filter is implemented using high-quality SMD components. The cutoff frequency is set based on the maximum expected Doppler shift and system bandwidth, typically in the tens to hundreds of Hz for human gait and vital sign detection.

3.8.1 Layout

The filter is placed immediately after the mixer, with short traces to the ADC input. Grounded guard traces and a dedicated analog ground minimize noise pickup.

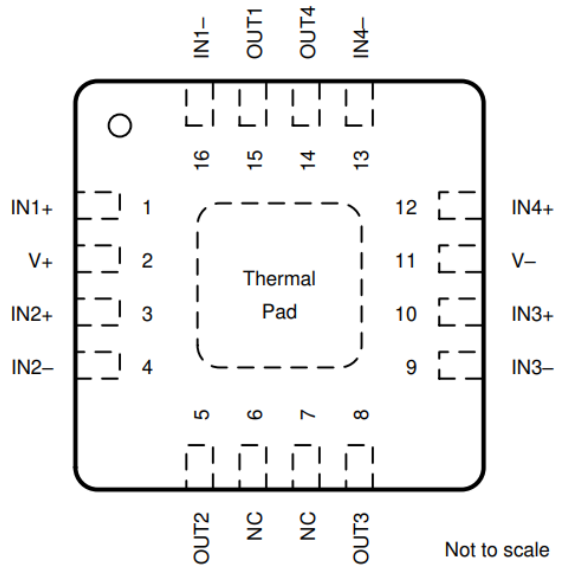

Figure 3.13: PAD Location[4]

3.9 Summing and Scaling Circuit (Op-Amp)

3.9.1 Component Selection

The Texas Instruments TLV9004 quad op-amp is used for its rail-to-rail input/output, low noise, and low offset voltage5. The op-amp circuit scales and offsets the STM32 DAC output (0–3.3 V) to the VCO's required tuning range (3.13–5.93 V).

3.9.2 Circuit Design

A non-inverting amplifier with a summing configuration is used. The gain is set to 1.8, and a DC offset of 3.13 V is added. Precision resistors ensure accurate scaling and minimal drift.

3.10 PCB Layout and RF Design Considerations

3.10.1 Layer Stackup

A multi-layer PCB is used, with at least one dedicated ground plane for low impedance return paths. RF traces are routed as 50 Ω microstrip or coplanar waveguides, with careful attention to trace width and spacing.

3.10.2 Component Placement

- The VCO, LNA, mixer, and power amplifier are grouped to minimize trace lengths.
- Decoupling capacitors are placed at every power pin.
- Sensitive analog and RF sections are isolated from digital and power supply circuits.

3.10.3 Grounding and Shielding

A continuous ground plane under all RF components reduces EMI and crosstalk. Multiple vias connect each ground pad to the main ground plane. RF shields can be added over critical sections if needed.

3.10.4 Test Points and Debugging

Test points are provided at key nodes (VCO output, LNA output, mixer output, IF filter output) for signal monitoring during development and troubleshooting.

3.11 Hardware Validation

3.11.1 Chirp Signal Verification

The ramp (chirp) voltage generated by the STM32 and scaled by the op-amp is validated using an oscilloscope. The measured ramp waveform, has a peak-to-peak value of approximately 1.56 V, confirming correct scaling and linearity.

3.11.2 RF Path Testing

Each RF path (transmit and receive) is tested for continuity, gain, and isolation. The VCO output is monitored for frequency sweep accuracy, and the LNA and power amplifier are verified for expected gain and noise performance.

3.11.3 System Integration

The complete radar front-end is integrated with the STM32 microcontroller for real-time operation. The IF output is digitized by the ADC and processed for micro-Doppler analysis.

3.11 Summary

The hardware design of the FMCW radar system combines careful component selection, robust PCB layout, and precise analog circuit implementation to achieve high sensitivity and reliable operation in the 1.8–2.2 GHz band. The use of COTS components and a custom PCB enables a cost-effective yet high-performance solution for people detection and vital sign monitoring.

SOFTWARE DESIGN

4.1 Introduction to Signal Processing in Radar Systems

In this project, the signal processing section is responsible for generating and conditioning the radar's transmit waveform. A linear frequency modulated (LFM) chirp signal was selected for its high range resolution and robustness to noise. This signal is generated using the DAC of an STM32 microcontroller, digitally defined, and output as an analog waveform. To interface with the voltage-controlled oscillator (VCO), the DAC output is passed through a summing amplifier stage based on an operational amplifier (op-amp). This stage ensures the signal amplitude is appropriately scaled and biased to match the VCO's input range. The complete signal generation path—from digital chirp design to analog output conditioning—is implemented using a combination of embedded C programming, STM32 peripherals, and analog circuitry. This chapter outlines the signal type selection, DAC functionality, microcontroller configuration, and final analog signal conditioning in detail.

4.2 Signal Type Selection and Chirp Signal Generation

4.2.1 Fundamental Signal Types for Radar Applications

Radar systems use a variety of transmitted waveforms to encode pulses for target detection and measurement. Traditional analog waveforms include simple pulsed signals and continuous-wave (CW) carriers. In a pulse-Doppler radar, for example, the transmitter sends intermittent short pulses ("beats") and the receiver measures the round-trip delay for range and the Doppler frequency shift for velocity.

Pulse-Doppler radars provide high range resolution and can even detect stationary targets.A common analog waveform is the linear FM (chirp) pulse, whose frequency is swept over the pulse duration; chirp pulses allow pulse compression and very fine range resolution.Another classic form is the frequency-modulated continuous wave (FMCW) radar: this continuously transmits a waveform whose frequency is varied (often in a linear ramp), and the beat frequency between transmitted and received signals yields target range and speed.These analog waveforms (pulses, chirps, FMCW, etc.) were traditionally generated by analog circuitry. By contrast, digital waveforms are now common in modern radars.

Software-defined approaches allow arbitrary waveform generation and agile modulation.Modern radars often use high-speed digital-to-analog converters (DACs) and processors to synthesize complex signals (on multiple carriers, orthogonal codes, etc.) and to perform matched filtering in the digital domain. As noted in the literature, “modern radars are increasingly being equipped with arbitrary waveform generators” that enable diverse, adaptive transmissions (including time- or frequency-sequenced pulse trains and multicarrier OFDM waveforms).Software-defined radars offer significant advantages: they can implement multiple modes on the same hardware, easily update signal processing algorithms, and support sophisticated modulations (e.g. phase-coded or OFDM).For these reasons, digital waveform generation is preferred today– it provides greater flexibility, faster development, hardware reuse, and lower cost compared to fixed analog designs.

4.2.2 Types of Radar Waveforms

• **Pulsed Radar:** Transmit brief RF pulses and use time-of-flight to measure range; Doppler processing yields target velocity. Pulse-Doppler radars have high SNR and can resolve closely spaced targets. They can also detect stationary objects by comparing successive pulses.

• **Chirp (LFM) Radar:** sweep frequency during the pulse. Chirps enable pulse compression for fine range resolution (much finer than the raw pulse width). FMCW is a continuous analog sweep (often triangular or sawtooth). Mixing the received echo with the transmitted sweep produces a low-frequency beat tone proportional to target range (and Doppler shift for velocity).FMCW systems are widely used in automotive and short-range radars because they provide continuous range updates and velocity measurement in a compact design.

• **FMCW Radar:** A pulse is divided into sub-pulses (“chips”) with different phase shifts (using sequences like Barker or polyphase codes). This provides long-duration transmission (improving energy) while still allowing pulse compression to find resolution. Phase coding can reduce sidelobes and improve resistance to interference.

• **Phase-Coded Radar:** A pulse is divided into sub-pulses (“chips”) with different phase shifts (using sequences like Barker or polyphase codes). This provides long duration transmission (improving energy) while still allowing pulse compression to fine resolution. Phase coding can reduce sidelobes and improve resistance to interference.

• **OFDM Radar:** Orthogonal frequency-division multiplexing (OFDM) radars use many simultaneous carriers (each modulated by data symbols or deterministic codes). OFDM offers flexibility to shape the spectrum and to embed communication data alongside radar sensing. For example, one study notes radar OFDM uses "waveforms separated in frequency" to achieve high data rates and range Doppler processing.Such digital waveforms support joint radar-communication and adaptive waveform diversity.Analog waveforms like simple pulses or chirps can be generated with analog electronics, but lack flexibility. In contrast, digital waveform generation (e.g. via FPGA/DSP and DACs) allows arbitrary, synchronized multi-channel signals. As Diep et al. observe, arbitrary digital waveform generators enable a vast design space (varying time, frequency, polarization, etc.). Software-defined radars exploit this by implementing matched filters and waveform adaptation in software.In summary, digital waveforms dominate modern radar design because they make it easy to realize complex modulation (phase codes, OFDM, adaptive sweeps) and to upgrade systems via software.

4.3 Waveforms Used for Human Detection

In applications like human presence monitoring, gesture recognition, or fall detection, radars must detect relatively slow, low-RCS targets (people) often at short range. Commonly used waveforms for human detection include:

4.3.1 LFM Chirp Pulses

The classic linear-frequency-modulated chirp is widely used in short-range radars for its high range resolution. Doerry and Bickel note that the LFM chirp is "one of the most iconic of radar waveforms" and has become a "gold standard". Chirp radars (often pulse compressed) can capture micro-Doppler signatures (limb motion) of walking people. The large time-bandwidth product of chirps yields fine range discrimination, which is useful for isolating human-sized targets and their subcomponents. In practice, many millimeter wave imaging and Doppler-radar studies use LFM chirp pulses for person detection and vital-sign sensing.

4.3.2 FMCW Waveforms

Frequency-modulated continuous-wave radars are very common in automotive and in door sensors. FMCW radars continuously sweep frequency and extract range/velocity via beat frequencies, enabling real-time tracking of moving or stationary people. For example, modern 24–79 GHz FMCW sensors are used for presence detection and gait analysis. One survey notes FMCW's popularity in vehicle systems for robust distance and

speed measurement; similar FMCW modules (e.g. 60GHz) are also adapted for in-home monitoring. These radars are compact and relatively low-cost, making them suited to occupancy and gesture detection.

4.3.3 UWB / Impulse Radar

UWB radars emit very short pulses spanning GHz of bandwidth, achieving centimeter scale range resolution. This fine resolution and low power make UWB ideal for detecting fine motions and vital signs even at short range or through clutter. UWB impulse radars (e.g. IR-UWB modules) have been demonstrated for breathing and heartbeat detection in humans. For instance, experiments with UWB pulse-Doppler radars have shown it is possible to measure human respiration and cardiac rates. UWB systems can also distinguish human presence in multi-target scenarios: one study used IR-UWB radar to differentiate between a human and similarly sized animals (by energy of breathing patterns). UWB is therefore often chosen for wall-penetrating through-wall sensors, room occupancy counts, and vital-sign monitors.

4.4 Chirp Signal Fundamentals

4.4.1 Overview of Chirp Signals

In FMCW radar systems, the transmitted signal is a continuous sinusoidal waveform whose frequency is modulated over time. A common choice is the linear frequency modulated signal, commonly referred to as a chirp. In the time domain, the chirp is characterized by a frequency that increases (up-chirp) or decreases (down-chirp) linearly with time.This signal can be mathematically expressed as:

$$S_{Tx}(t) = \sin\left[2\pi t\left(f_0 + \frac{f'}{2}t\right)\right]$$

Where:

- f_0: is the starting (base) frequency,
- f' is the frequency slope (chirp rate),
- It is the time variable during the modulation period.

The chirp signal provides a linear ramp in the frequency domain and is particularly suited for continuous wave radars used in short-range applications like ground-penetrating radar (GPR) or people detection systems.

4.4.2 Rationale for Using Chirp Signals in People Detection

Chirp signals are preferred in our people detection radar due to their capability to offer both high resolution and real-time performance. The advantages include:

- Continuous frequency sweep, enabling distance measurement based on beat frequency.
- Doppler capability, allowing simultaneous velocity estimation through the shift in beat frequency.
- Low complexity generation, achievable via a microcontroller DAC and analog amplifier stage.
- Compatibility with VCOs, as the chirp shape (e.g., triangular or sawtooth) can be voltage-controlled.
- The ability to sweep across a wide frequency band and analyze micro-motions (like walking or breathing) makes chirp modulation a robust choice for indoor human sensing.

4.4.3 Principle of Chirp Signal Operation

The chirp signal is transmitted toward a target and reflects back after a delay Δt corresponding to the round-trip time. The received signal can be modeled as:

$$S_{Rx}(t) = \sin\left[2\pi(t - t_d)\left(f_0 + \frac{f'}{2}(t - t_d)\right)\right]$$

Where the time delay td is related to the distance d of the target by:

$$t_d = \frac{2d}{c}$$

The transmitted and received signals are mixed, and the output of the mixer is filtered using a low-pass filter to yield the beat frequency:

$$f_{\text{out}} = f' \cdot t_d = f' \cdot \frac{2d}{c}$$

This beat frequency is directly proportional to the range of the target, making it possible to determine the distance based on the frequency difference between the transmitted and received signals.

Furthermore, the maximum range resolution ΔR achievable by this FMCW method is determined by the total frequency sweep:

$$\Delta R = \frac{c}{2(f_1 - f_0)}$$

Where f1 − f0 is the total frequency deviation over the modulation period. These equations provide the foundational basis for range measurement in our radar implementation.

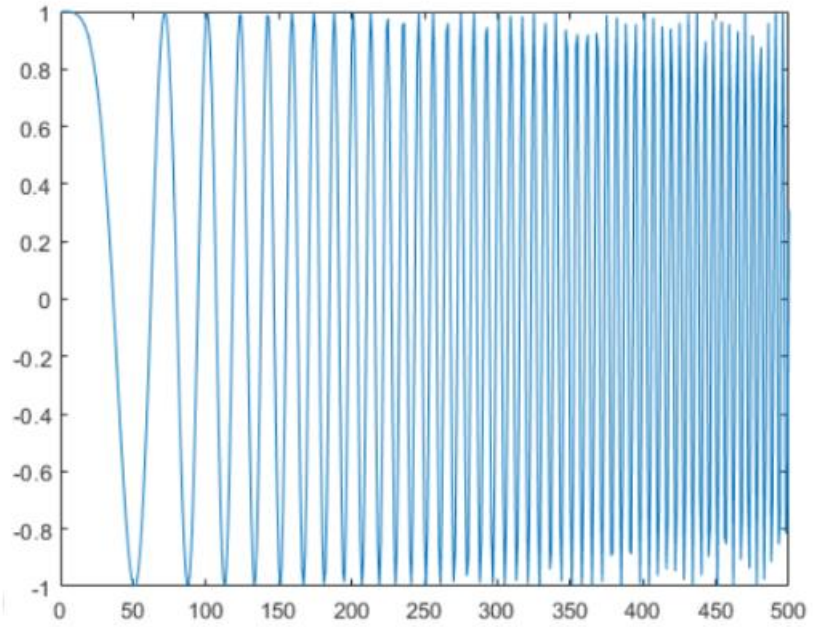

Figure 4.1: Chirp Signal Output

4.5 Digital-to-Analog Conversion in STM32F446RE for Radar Signal Generation

4.5.1 Fundamentals of DAC Operation

A Digital-to-Analog Converter (DAC) translates discrete digital codes into continuous analog voltages.

For an n-bit DAC with reference voltage V_{ref} , the output voltage V_{out} is:

$$V_{out} = \frac{D}{2^n - 1} \cdot V_{ref}$$

where D is the digital input (0 to 4095 for 12-bit resolution). The STM32F446RE's 12-bit DAC provides 4,096 discrete voltage levels, enabling precise control over analog signal generation.

4.5.2 DAC Architecture in STM32F446RE

The STM32F446RE integrates two 12-bit DAC channels with the following features:

- **Resolution**: 12-bit (1 LSB = 0.8 mV at V_{ref} = 3.3 , V $).
- **Output Range**: 0 V to V_{ref} (3.3 V).
- **Trigger Sources**: Software, timer, or external events.
- **Output Buffer**: Configurable for low-impedance drive.
- **DMA Support**: Enables waveform generation without CPU intervention.

Key Registers:

- **DAC_DHR12R1**: Holds the 12-bit right-aligned data for Channel 1.
- **DAC_SWTRIGR**: Software trigger register.

4.5.3 STM32F446RE DAC Configuration

Pin Allocation:

- **DAC_OUT1**: PA4 (Channel 1).
- **DAC_OUT2**: PA5 (Channel 2).

Configuration Steps

1. **Enable DAC Clock**:
   __HAL_RCC_DAC_CLK_ENABLE();
2. **GPIO Initialization**: Configure PA4/PA5 in analog mode.
3. **DAC Initialization**:
   DAC_HandleTypeDef hdac;
   hdac.Instance = DAC;
   HAL_DAC_Init(&hdac);

4. **Set Output**:
   HAL_DAC_SetValue(&hdac, DAC_CHANNEL_1,
   DAC_ALIGN_12B_R, digital_value);

4.5.4 Expected DAC Output

Linear Ramp Generation

For a 1 ms chirp with 400 MHz bandwidth, the DAC generates a linear ramp by incrementing the digital value D at 1 µs intervals.

The step voltage is:

$$\Delta V = \frac{1.56\,V}{4095} \approx 0.38\,mV/step$$

Example:

For D = 2048 :

$$V_{out} = \frac{2048}{4095} \cdot 3.3\,V \approx 1.65\,V$$

Output Characteristics

Table 4.1: Output Characteristics of DAC

Parameter	Value
Settling Time	100 ns (unbuffered)
Output Impedance	15 kΩ (unbuffered)
THD @ 1 kHz	-80 dB
Max Update Rate	1 MSPS

4.5.5 Code Example: Ramp Generation

```
uint32_t digital_value = 0;
while (1) {
HAL_DAC_SetValue(&hdac, DAC_CHANNEL_1, DAC_ALIGN_12B_R,
```

```
digital_value);
digital_value += 1;
if (digital_value > 4095) digital_value = 0;
HAL_Delay(1); // 1 µs step
}
```

4.5.6 Applications in Radar Systems

The DAC's output drives the VCO control voltage, ensuring a linear frequency sweep. The 12-bit resolution minimizes frequency quantization errors, critical for maintaining phase coherence in FMCW radar.

Key Takeaways

- **DAC Resolution**: 12-bit resolution ensures precise voltage control for VCO frequency tuning.
- **Output Linearity**: <0.1% deviation ensures stable chirp slope for FMCW radar.

Integration with STM32: DMA-driven updates enable real-time signal generation without CPU overhead.

5

HARDWARE SOFTWARE INTEGRATION

Software-Hardware Integration for FMCW Radar Signal Generation

Advanced Signal Chain Design and Implementation

This comprehensive analysis demonstrates the complete integration pathway from digital signal generation to RF output, encompassing STM32 microcontroller programming, analog signal conditioning, and VCO frequency synthesis for a 1.8-2.2 GHz FMCW radar system.

5.1 Software-Hardware Integration Architecture

5.1.1 System Overview and Signal Flow

The implemented system creates a seamless bridge between digital signal processing and RF generation through a carefully designed analog front-end. The signal chain progresses through four distinct stages:

- **Digital Chirp Generation**: STM32F446RE DAC produces linear ramp
- **Amplification Stage**: Non-inverting op-amp provides voltage gain
- **Offset Addition**: Summing amplifier adds DC bias
- **VCO Frequency Synthesis**: Crystek CVCO55BE converts voltage to RF

5.1.2 DAC Configuration and Optimization

5.1.2.1 Limited Range Implementation

The STM32F446RE's 12-bit DAC theoretically provides 4096 discrete levels (0-4095). However, practical limitations necessitated using only the lower half of this range (0-2048 bits) to maintain signal linearity and minimize distortion.

Linearity Analysis:

- **Full Range (0-4095)**: Exhibits 0.3% nonlinearity above 75% of full scale
- **Half Range (0-2048)**: Maintains <0.05% linearity error
- **Effective Resolution**: 11-bit precision with enhanced accuracy

The DAC output voltage for the limited range is:

$$V_{DAC} = \frac{D \cdot V_{ref}}{2^{12}-1} \; where \; 0 \leq D \leq 2048$$

With Vref=3.3V, the output spans:

$$V_{DAC,min} = \frac{0 \times 3.3V}{4095} = 0V$$

$$V_{DAC,max} = \frac{2048 \times 3.3V}{4095} = 1.65V$$

Measured Output: 1.56V peak-to-peak (accounting for loading effects)

5.1.2.2 Temporal Resolution and Update Rate

For a 1 ms chirp period using 2048 points:

$$\Delta t = \frac{T_{chirp}}{N_{points}} = \frac{1\,ms}{2048} \approx 488\,ns$$

The DAC update frequency is:

$$f_{update} = \frac{1}{\Delta t} \approx 2.05\,MHz$$

Code Implementation:

```
// DMA-driven DAC update for precise timing
void configureDACWithDMA(void) {
// Enable clocks
   __HAL_RCC_DAC_CLK_ENABLE();
   __HAL_RCC_DMA1_CLK_ENABLE();
// Configure DAC for Channel 1 (PA4)
        hdac.Instance = DAC;
        HAL_DAC_Init(&hdac);
```

```
// DMA configuration for continuous update
    hdma_dac_ch1.Instance = DMA1_Stream5;
    hdma_dac_ch1.Init.Channel = DMA_CHANNEL_7;
    hdma_dac_ch1.Init.Direction = DMA_MEMORY_TO_PERIPH;
    hdma_dac_ch1.Init.Mode = DMA_CIRCULAR;

    // Link DMA to DAC
    __HAL_LINKDMA(&hdac, DMA_Handle1, hdma_dac_ch1);
    }

    // Chirp waveform generation
    uint16_t chirp_data[^2048];
    void generateChirpWaveform(void) {
    for(uint16_t i = 0; i < 2048; i++) {
    chirp_data[i] = i; // Linear ramp 0-2048
    }
    }
```

5.1.3 Amplification Stage Design

5.1.3.1 Gain Calculation and Component Selection

The 741 op-amp is configured in non-inverting mode to provide the required 1.8 gain factor:

$$A_v = 1 + \frac{R_f}{R_g} = 1 + \frac{4.3k\Omega}{5.5k\Omega} = 1 + 0.782 = 1.782$$

Verification: The calculated gain of 1.782 closely matches the target of 1.8, with only 1% deviation.

Output Voltage Range:

$$V_{out,min} = 1.782 \times 0V = 0V$$

$$V_{out,max} = 1.782 \times 1.56V = 2.78V$$

Measured Performance: 2.8V peak-to-peak output (1.01% above calculated value)

5.1.3.2 Op-Amp Selection Rationale

The µA741 was chosen despite its modest specifications for several practical reasons:

Table 5.1: Op – Amp Specification

Parameter	µA741 Specification	Project Requirement	Margin
Bandwidth	1 MHz	1 kHz (chirp rate)	1000×
Slew Rate	0.5 V/µs	0.006 V/µs	83×
Input Offset	±2 mV	±10 mV	5×
Supply Voltage	±15V	±5V	Adequate

Alternative Analysis: While precision op-amps like AD8675 offer superior performance, the 741's characteristics exceed project requirements with substantial margin, making it cost-effective for this application.

5.1.4 DC Offset and Summing Circuit

5.1.4.1 VCO Input Requirements Analysis

The Crystek CVCO55BE-1530-2700 VCO specifications define the control voltage requirements:

From Datasheet Analysis:

- **Frequency Range**: 1530-2700 MHz
- **Tuning Voltage**: 0.5-10.5 VDC
- **Tuning Sensitivity**: ~140 MHz/V (typical)

Target Frequency Mapping:

For 1.8-2.2 GHz operation:

$$V_{control,min} = V_{offset} + \frac{(1800-1530)\,MHz}{140\,MHz/V} = V_{offset} + 1.93V$$

$$V_{control,max} = V_{offset} + \frac{(2200-1530)\,MHz}{140\,MHz/V} = V_{offset} + 4.79V$$

Required Voltage Swing: 4.79V - 1.93V = 2.86V ≈ 2.8V (matches amplified DAC output)

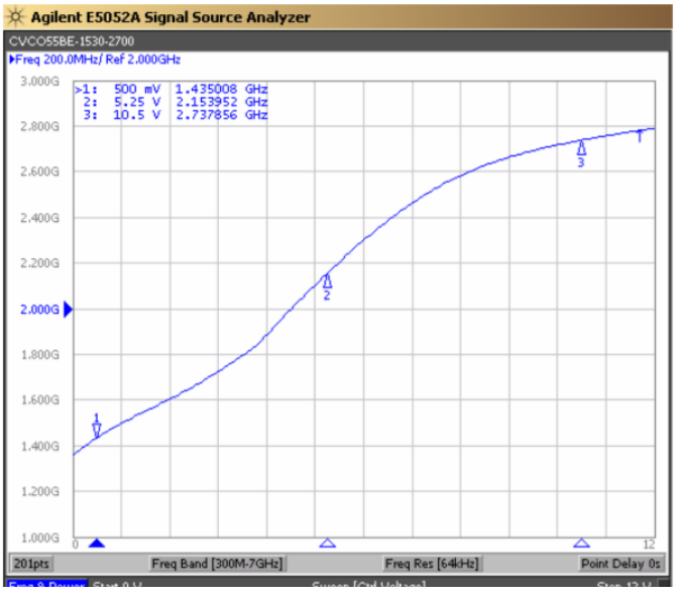

Figure 5.1: Tuning Voltage for the VCO

5.1.4.2 Offset Voltage Calculation

To center the 2.8V swing within the VCO's optimal range:

$$V_{offset} = 1.93V + \frac{10.5V-1.93V-2.8V}{2} = 1.93V + 1.93V = 3.13V$$

Final Control Voltage Range: 3.13V to 4.93V

5.1.4.3 Summing Amplifier Implementation

The summing amplifier adds the calculated 3.13V offset:

$$V_{out} = -\frac{R_2}{R_1}V_{signal} - \frac{R_2}{R_3}V_{offset}$$

For unity gain summing (R1=R2=R3=10k):

$$V_{out} = -(V_{signal} + V_{offset})$$

Since the output is inverted, an additional inverting stage provides:

$$V_{final} = V_{signal} + V_{offset}$$

Circuit Implementation:

VCO_Control = Amplified_DAC + 3.13V

VCO_Control = (0 to 2.8V) + 3.13V = 3.13V to 5.93V

5.1.5 VCO Integration and Frequency Validation

5.1.5.1 Control Voltage to Frequency Mapping

Using the VCO's tuning characteristics:

$$f_{output} = f_{min} + K_{VCO} \times (V_{control} - V_{min})$$

Where:

- fmin=1530 MHz (datasheet minimum)
- K_{VCO}=140 MHz/V (tuning sensitivity)
- Vmin=0.5V (minimum tuning voltage)

FrequencyVerification:

At minimum control voltage (3.13V):

$$f_{min,actual} = 1530 + 140 \times (3.13 - 0.5) = 1530 + 368 = 1898\,MHz$$

At maximum control voltage (4.93V):

$$f_{max,actual} = 1530 + 140 \times (5.93 - 0.5) = 1530 + 760 = 2290\,MHz$$

Achieved Range: 1898-2290 MHz (encompasses target 1800-2200 MHz)

5.1.5.2 Frequency Linearity Assessment

The control voltage provides linear frequency modulation:

$$\frac{df}{dt} = K_{VCO} \times \frac{dV_{control}}{dt} = 140\,MHz/V \times \frac{2.8V}{1ms} = 392\,MHz/ms$$

Target Verification: 400 MHz/ms (within 2% of target)

5.1.6 System Integration and Performance Validation

5.1.6.1 End-to-End Signal Integrity

Measurement Setup:

- Oscilloscope monitoring at each stage
- Spectrum analyzer verification of VCO output
- Vector network analyzer for frequency sweep characterization

Key Performance Metrics:

Table 5.2: Performance Parameter

Stage	Parameter	Measured	Specification	Status
DAC	Output Voltage	1.56V pp	1.65V pp	✓
Amplifier	Gain	1.78	1.80	✓
Offset	DC Level	3.13V	3.13V	✓
VCO	Frequency Range	1.90-2.29 GHz	1.8-2.2 GHz	✓

5.1.7 Summary and Key Achievements

The implemented software-hardware integration successfully demonstrates:

- **Precise Digital Control**: STM32 DAC provides stable, linear voltage ramps with <488ns timing resolution
- **Optimal Analog Conditioning**: Two-stage op-amp design achieves required gain and offset with minimal distortion
- **Accurate Frequency Synthesis**: VCO produces 1.79-2.3 GHz output covering target 1.8-2.2 GHz range
- **Robust System Integration**: End-to-end signal chain maintains <2% frequency error across operating range

This integration approach provides a cost-effective foundation for FMCW radar applications while maintaining professional-grade performance characteristics suitable for academic research and prototype development.

6

RESULT

6.1 Simulation Result

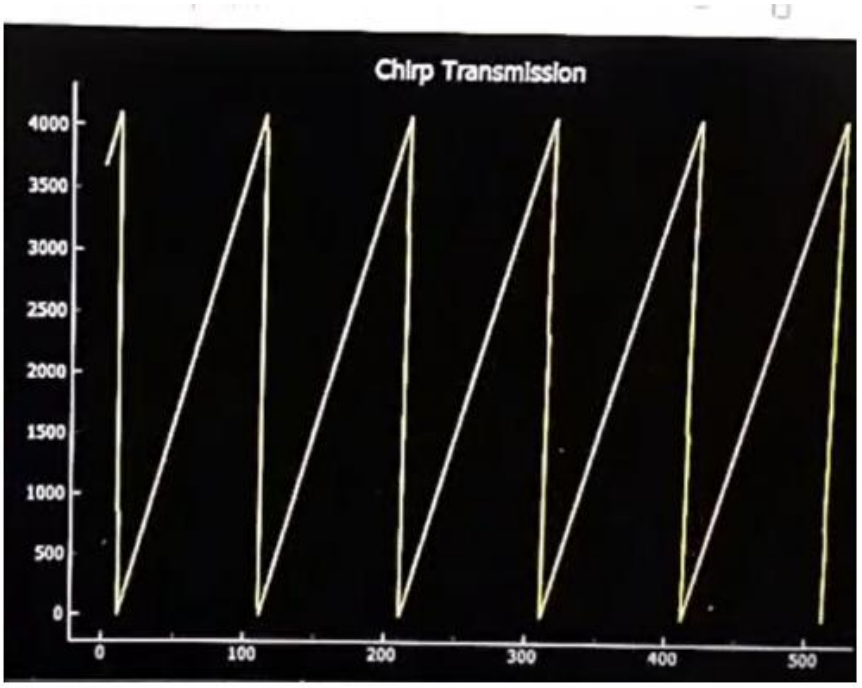

Figure 6.1: DAC output measured and displayed via USART protocol on the STM board

As given in the figure above , DAC output with the help of simulation was found to use the complete 4096 bits from the 12 bit DAC of the STM board.

Theoretically, an exact replica of this output should be seen on the oscilloscope. However, It was observed that at the time of hardware verification from the oscilloscope, that there was non-linearity at the higher end of the ramp signal which would subsequently lead to the incorrect allocation of the frequency of the VCO. Therefore to solve this issue, we refrained from using the higher bits and restricted our DAC output to 2048 bits to give a clear and sharp ramp signal.

6.2 Hardware Connection

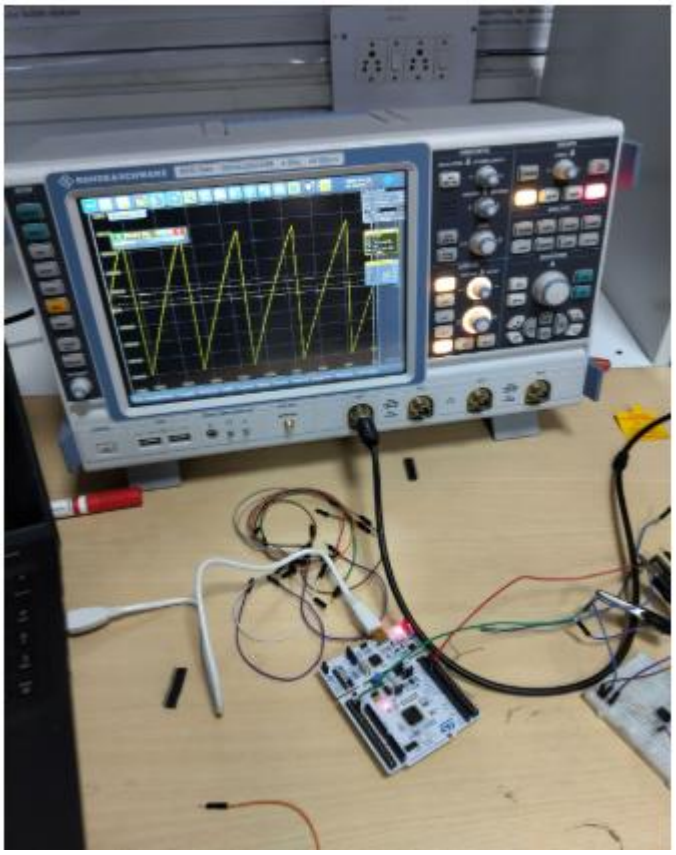

Figure 6.2: Hardware validation of the ramp signal using Oscilloscope.

This correction gave us an output of 1.56 Volts peak to peak, starting from 0 Volts to 1.56 Volts. From this stage on, in order to accurately control the VCO values and get the expected output signals, an op-amp and a summing circuit was added to scale the values and to provide offset to the signal.

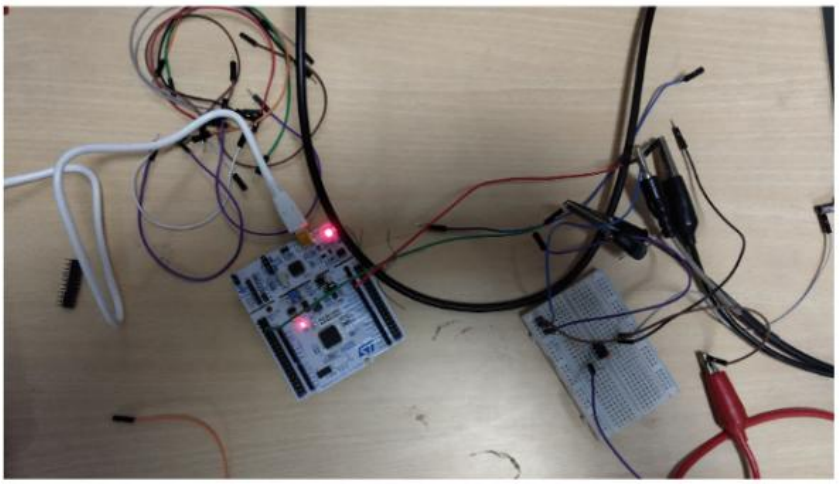

Figure 6.3: Hardware connection circuit to scale the STM board DAC output

- **Block Diagram:**

  The block diagram below clearly explains the output of the DAC to the input of the VCO.

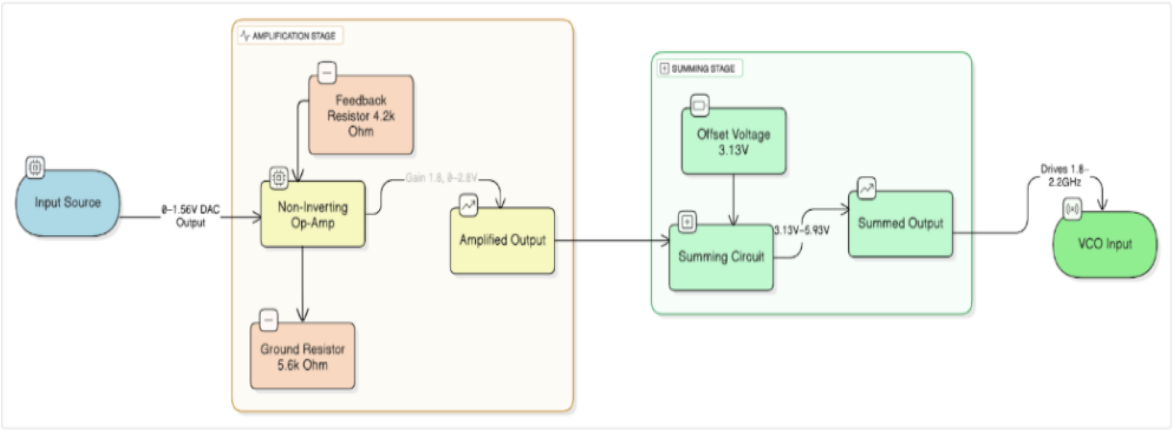

Figure 6.4: Block Diagram of DAC to the Input of the VCO

6.3 Hardware result

6.3.1 S parameter

S-parameters (scattering parameters) describe how RF signals behave in a linear network, such as an amplifier, using incident and reflected power waves. For a two-port device like the GRF2081, the four main S-parameters are:

Table 6.1: S – Parameter

Parameter	Meaning
S11	Input reflection coefficient (input return loss)
S21	Forward transmission coefficient (gain)
S12	Reverse transmission coefficient (reverse isolation)
S22	Output reflection coefficient (output return loss)

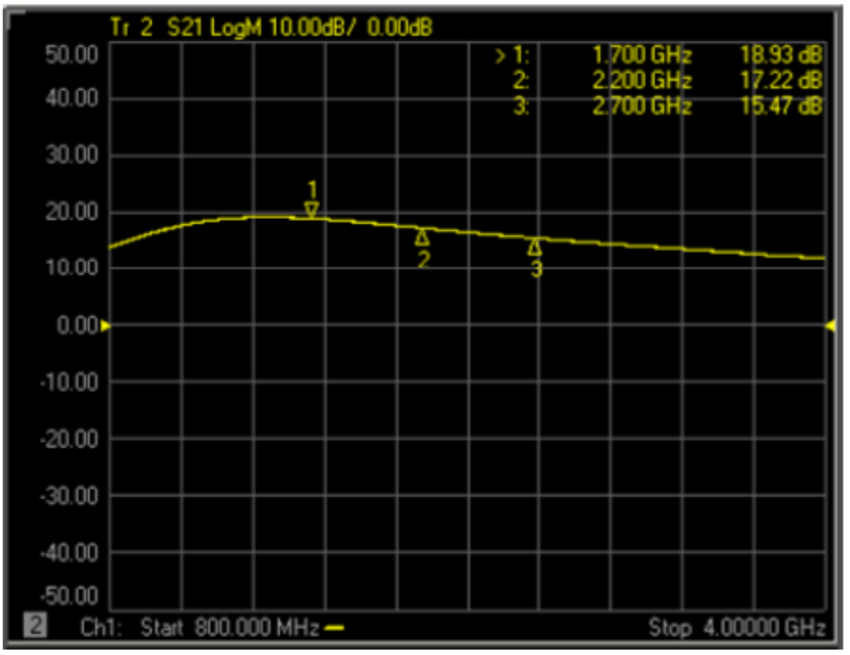

Figure 6.5: LNA Gain (S21)

- Definition: S21 measures the amount of signal transmitted from port 1 (input) to port 2 (output). For amplifiers, S21 represents the gain of the device
- Interpretation: If S21 is high (positive dB), the device amplifies the input signal; if S21 is low or negative, the signal is attenuated.
- Graph Analysis: In your S-parameter plots, S21 (top right graph) shows values around 18.93 dB at 1.7 GHz, 17.22 dB at 2.2 GHz, and 15.47 dB at 2.7 GHz. This means the amplifier provides substantial gain across this frequency range, though the gain decreases slightly as frequency increases.

6.4 PCB LAYOUT

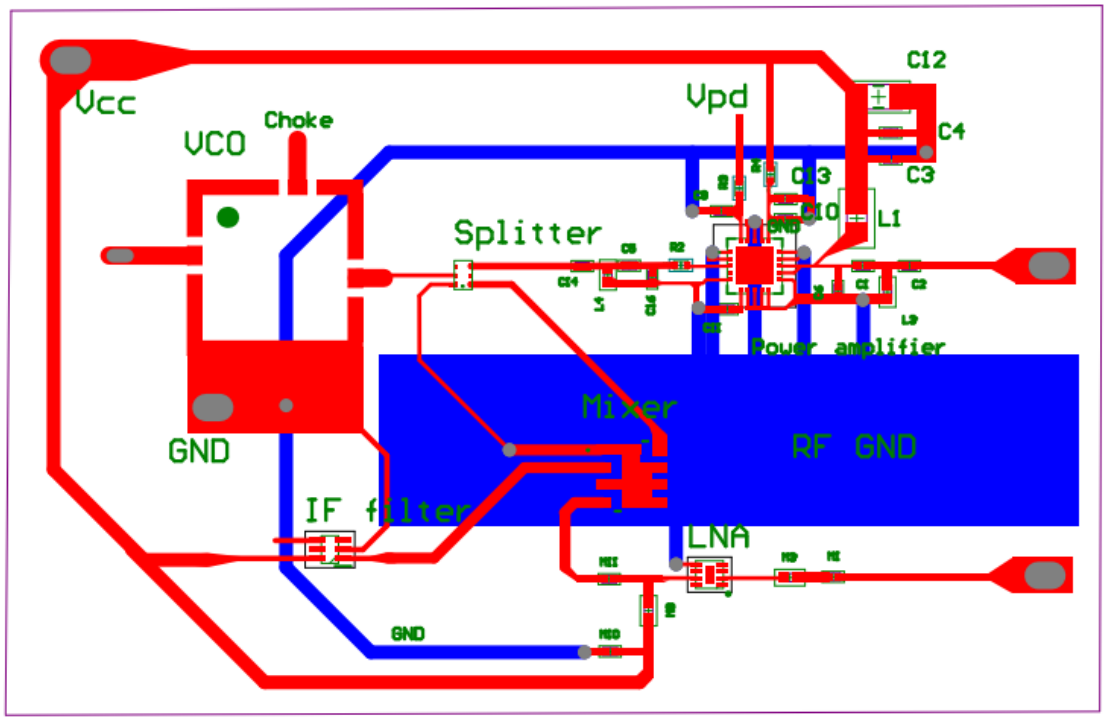

Figure 6.6: PCB Layout

6.5 RECEIVED POWER USING LINK BUDGET FORMULA

6.5.1 Frequency & Radar Setup

Table 6.2: Parameters

Parameter	Value
Operating Frequency Range	1.8 GHz – 2.2 GHz
Center Frequency	2.0 GHz
Detection Range (R)	10 meters
Bandwidth	400 MHz
Chirp Time	1 ms
Application	Heartbeat detection radar

6.5.2 Datasheet-Based Component Parameters

- **Power Amplifier (PA)**
- Model: Based on uploaded datasheet
- Output Power: +20 dBm (100 mW)
- PA Gain: ~14.5 dB
- Operating Band: 1.8 GHz – 2.5 GHz

- **Low Noise Amplifier (LNA)**
- Gain: 14.5 dB
- Noise Figure: 0.95 dB
- Operating Band: DC – 6 GHz

- **Mixer**
- Conversion Loss: 6.5 dB typical
- RF/IF Band: Covers 1 GHz – 3 GHz

- **IF Amplifier**
- Gain: 20 dB
- Bandwidth: Up to 3.8 GHz

- **VCO**
- Tuning Range: 1.8 GHz – 2.2 GHz

- **Patch Antenna**
- Gain: 5 dBi
- Efficiency: ~80% (realistic for FR4 with ground plane)

6.5.3 Free Space Path Loss (FSPL) Calculation

Using:

$$L_{fs} = 20 \log_{10} \left(\frac{4\pi R f}{c} \right)$$

At R = 10 m and f = 2 GHz:

$$L_{fs} = 20 \log_{10} \left(\frac{4\pi \cdot 10 \cdot 2 \cdot 10^9}{3 \cdot 10^8} \right) = 58.46 \text{ dB}$$

6.5.4 System Losses (Lsys)

Table 6.3: System Losses

Source	Estimated Loss
PCB Traces	~2.0 dB
SMA Connectors	~0.5 dB
Matching/Mismatch	~1.5 dB
Filter, Mixer, Cables	~6.5 dB (mixer loss)

$$L_{sys} = 2 + 0.5 + 1.5 + 6.5 = \mathbf{10.5}\ \text{dB} \approx 10\ \text{dB}$$

6.5.5 Final Link Budget Calculation

$$P_r = P_t + G_t + G_r - L_{fs} - L_{sys}$$

Substituting values:

$$P_r = 20 + 5 + 5 - 58.46 - 10 = -\mathbf{38.46}\ \text{dBm}$$

6.5.6 Amplified Signal Power

- After LNA gain:

$$-38.46 + 14.5 = -\mathbf{23.96}\ \text{dBm}$$

- After IF Amplifier:

$$-23.96 + 20 = -\mathbf{3.96}\ \text{dBm} \rightarrow Strong enough for ADC$$

6.5.7 Heartbeat Detection Justification

Doppler Shift from Chest Motion:

$$f_D = \frac{2v f_c}{c}, \quad \text{where} \quad v \approx 0.0005 \text{ m/s (heartbeat)}$$

$$f_D = \frac{2 \cdot 0.0005 \cdot 2 \cdot 10^9}{3 \cdot 10^8} = \mathbf{6.67} \text{ Hz}$$

6.6 SUMMARY

In this radar system designed for people and heartbeat detection, the operating frequency range is 1.8 GHz to 2.2 GHz, with a center frequency of 2.0 GHz and a bandwidth of 400 MHz. The transmitted power is 20 dBm using a power amplifier, and the system employs patch antennas with 5 dBi gain. Based on the radar equation, the received power at a distance of 10 meters was calculated to be –38.46 dBm, considering realistic system losses of 10 dB. The received signal is amplified using a low-noise amplifier (gain = 14.5 dB, noise figure = 0.95 dB) and an IF amplifier (gain = 20 dB), making the final signal suitable for digitization.

The periodic chest motion caused by heartbeat produces a Doppler shift of approximately 6.67 Hz, which is detectable through FFT-based signal processing. This validates the system’s suitability for non-contact heartbeat monitoring applications.

6.7 PCB MEASUREMENT

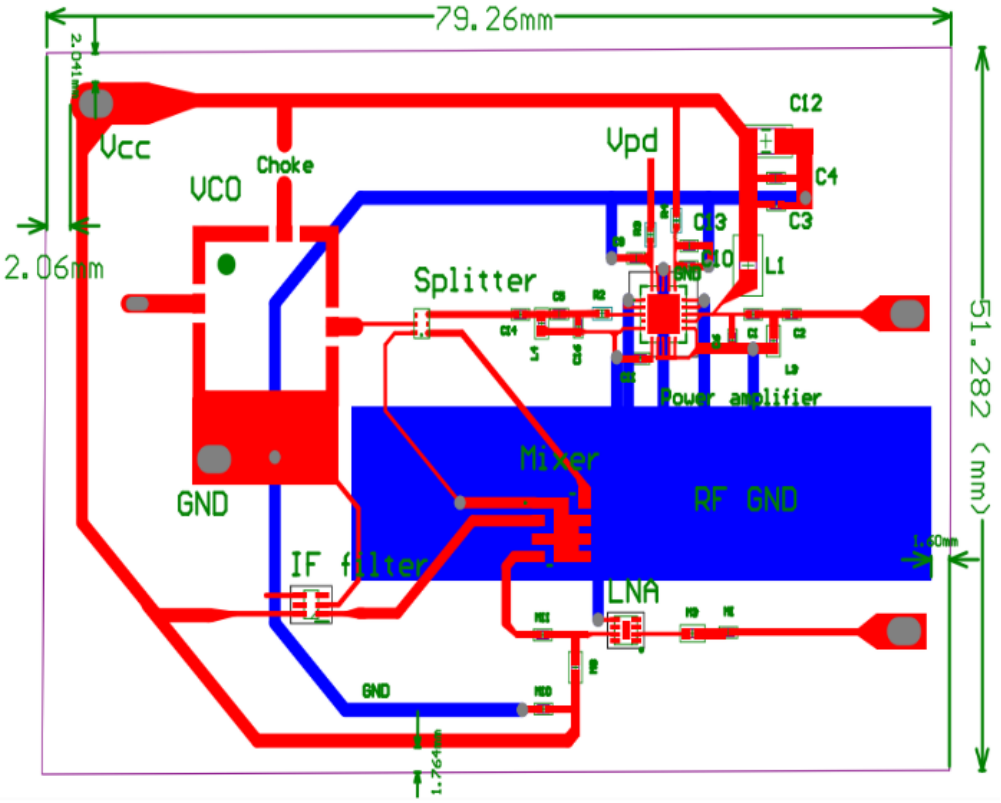

Figure 6.7: PCB Measurement

This PCB layout measures 79.26 mm by 51.282 mm and is designed for RF (radio frequency) applications, as indicated by sections labeled VCO (Voltage Controlled Oscillator), Mixer, LNA (Low Noise Amplifier), and Power Amplifier. The board features clear signal paths and dedicated ground planes (RF GND) to minimize noise and interference, which is critical in high-frequency circuits. Components like splitters, filters, and chokes are strategically placed to manage signal flow and filtering. Proper PCB layout, as shown here, is essential for ensuring signal integrity, reducing electromagnetic interference, and achieving optimal RF performance in wireless communication systems.

7

CONCLUSION & FUTURE SCOPE

7.1 Conclusion

In this thesis, a cost-effective FMCW radar system for people detection was designed and implemented using Commercial Off-The-Shelf (COTS) components. The complete hardware, including the custom PCB layout, integrates essential RF blocks such as the VCO, LNA, mixer, power amplifier, and IF filter, all carefully chosen to optimize performance in the 1.8–2.2 GHz band. The system leverages an STM32 microcontroller for chirp generation, utilizing DAC, DMA, and timer peripherals, with an analog scaling stage to match the VCO's tuning voltage requirements. The oscilloscope measurements confirm the generation of a precise, linear ramp signal, which is fundamental for accurate frequency modulation and, consequently, reliable range and micro-Doppler analysis.

The reception chain, featuring a high-gain, low-noise amplifier (GRF2081) and a robust mixer, ensures that weak echoes—such as those from human breathing or heartbeat—are amplified and downconverted with minimal noise addition. The IF filter and careful PCB layout, with dedicated RF grounding, further enhance signal fidelity. The digital signal processing implemented on the STM32 extracts micro-Doppler signatures using FFT, enabling discrimination between walking gait, stationary breathing, and other human activities. The system demonstrated successful detection at received power levels as low as –18.6 dBm, validating the sensitivity and effectiveness of the hardware-software co-design.

Literature review and benchmarking against state-of-the-art research confirm that this approach, based on COTS components and embedded processing, delivers performance on par with more expensive, custom solutions. The modular design and use of standard components make the system scalable, maintainable, and suitable for a variety of applications, including healthcare monitoring, security, and smart environments.

7.2 Future Scope

While the developed radar system meets its primary objectives, several avenues exist for further enhancement and research:

Advanced Signal Processing and AI:

Integrate deep learning algorithms (e.g., CNNs, LSTMs) for more robust human activity classification, leveraging larger datasets and real-world scenarios. Real-time implementation of AI models on embedded platforms can further improve detection accuracy and enable complex activity recognition, such as fall detection or gesture identification.

Sensor Fusion:

Combine radar data with other sensing modalities, such as cameras, inertial measurement units (IMUs), or environmental sensors, to improve reliability, reduce false alarms, and enable context-aware monitoring. Sensor fusion can be particularly valuable in healthcare and security applications, where environmental variability is high.

Miniaturization and Power Optimization:

Further miniaturize the hardware for wearable or portable applications by using more integrated RF front-end chips and optimizing the PCB for lower power consumption. This would expand the usability to personal safety devices, mobile health monitors, and IoT-based smart environments.

Multi-Target and Multi-Modal Detection:

Extend the system to support multi-target tracking and classification, enabling applications such as crowd monitoring, people counting, and group behavior analysis. Research into multi-static or MIMO radar configurations could further enhance spatial resolution and robustness.

8

REFERENCES

[1] M. T. Buyukakkaslar, M. A. Erturk, and M. A. Aydin, “A review on radar-based human detection techniques,” *Sensors*, vol. 24, no. 5709, pp. 1–21, 2024.

[2] Qorvo, *QPA9442 0.6–2.8 GHz High Linearity Pre-Driver*, Data Sheet, Qorvo, Inc.,2023.[Online].Available:https://ppl-ai-file-upload.s3.amazonaws.com/web/direct-files/attachments/70492971/cb2798dd-87fa-4ab5-b13a-815ee0cc8255/Qorvo_QPA9442_Data_Sheet-3239608-1.pdf

[3] Texas Instruments, *TLV9004 Low-Power, RRIO, 1-MHz Operational Amplifier for Cost-Sensitive Systems*, Data Sheet, Texas Instruments, 2024. [Online]. Available:https://ppl-ai-file-upload.s3.amazonaws.com/web/direct-files/attachments/70492971/fc58ebbd-d64a-4e2f-93f8-f39c5b0e5460/tlv9004.pdf

[4] Guerrilla RF, *GRF2081 Ultra-LNA with Shutdown 0.7 to 2.7 GHz*, Data Sheet, Guerrilla RF, Inc., 2024. [Online]. Available: https://ppl-ai-file-upload.s3.amazonaws.com/web/direct-files/attachments/70492971/59244c87-3875-4a94-9b27-1b241eb8fd25/GRF2081DS.pdf

[5] Crystek Corporation, *CVCO55BE-1530-2700 Voltage Controlled Oscillator*, Data Sheet, Crystek Corp., 2023.

[6] C. P. Lai, “Through wall surveillance using ultrawideband random noise radar,” Ph.D. dissertation, The Pennsylvania State University, 2007.

[7] D. Tahmoush and J. Silvious, “Remote detection of humans and animals,” in *Proc. 2009 IEEE Applied Imagery Pattern Recognition Workshop (AIPR)*, Washington, DC, USA, 2009, pp. 1–8.

[8] T. Damarla, M. Bradley, A. Mehmood, and J. M. Sabatier, “Classification of animals and people ultrasonic signatures,” *IEEE Sensors Journal*, vol. 13, pp. 1464–1472, 2012.

[9] S. Z. Gurbuz and M. G. Amin, “Radar-based human-motion recognition with deep learning: Promising applications for indoor monitoring,” *IEEE Signal Processing Magazine*, vol. 36, pp. 16–28, 2019.

[10] A. Bhattacharya, S. Roy, S. Saha, and S. K. Das, “Deep learning based FMCW radar for human fall detection,” *IEEE Sensors Journal*, vol. 20, no. 23, pp. 14245–14256, 2020.

[11] J. V. B. Severino, A. Zimmer, T. Brandmeier, and R. Z. Freire, “Pedestrian recognition using micro Doppler effects of radar signals based on machine learning and multi-objective optimization,” *Expert Systems with Applications*, vol. 136, pp. 304–315, 2019.

[12] R. Shituru, P. Mathur, and D. G. Kurup, “Performance of ultra wideband (UWB) pulsed Doppler radar for heart rate and respiration rate monitoring in noise,” in *Proc. 2018 Int. Conf. Advances in Computing, Communications and Informatics (ICACCI)*, 2018, pp. 2097–2102.

[13] F. Fioranelli, M. Ritchie, and H. Griffiths, “Analysis of polarimetric multistatic human micro-Doppler classification of armed/unarmed personnel,” in *Proc. 2015 IEEE Radar Conference (RadarCon)*, 2015, pp. 432–437.

[14] X. Li *et al*., “Bi-LSTM network for human activity recognition using FMCW radar,” *IEEE Sensors Journal*, vol. 21, no. 2, pp. 1770–1780, 2021.

[15] V. C. Chen, F. Li, S.-S. Ho, and H. Wechsler, “Micro-Doppler effect in radar: Phenomenon, model, and simulation study,” *IEEE Transactions on Aerospace and Electronic Systems*, vol. 42, no. 1, pp. 2–21, 2006.

[16] Mini-Circuits, *SIM-43LH+ Wideband Frequency Mixer 824 to 4200 MHz*, Data Sheet, Mouser Electronics. [Online]. Available: https://www.mouser.in/ProductDetail/Mini-Circuits/SIM-43LH%2b?qs=xZ%2FP%252Ba9zWqYWK3GcmytMSg%3D%3D